Optical Society of America. Anbo Wang, Mark S. Miller, Angela J. Plante, Michael F. Gunther, Kent A. Murphy, and Richard O. Claus, "Split-spectrum intensity-based optical fiber sensors for measurement of microdisplacement, strain, and pressure," Appl. Opt. 35, 2595-2601 (1996). doi: 10.1364/ao.35.002595

Split-spectrum intensity-based optical fiber sensors for measurement of microdisplacement, strain, and pressure

Anbo Wang, Mark S. Miller, Angela J. Plante, Michael F. Gunther, Kent A. Murphy, and Richard O. Claus

A self-referencing technique compensating for fiber losses and source fluctuations in reflective air-gap intensity-based optical fiber sensors is described. A dielectric multilayer short-wave-pass filter is fabricated onto or attached to the output end face of the lead-in–lead-out multimode fiber. The incoming broadband light from a white light or a light-emitting diode is partially reflected at the filter. The transmitted light through the filter projects onto a mirror. The light returning from the reflecting mirror is recoupled into the lead-in–lead-out fiber. These two reflections from the filter and the reflecting mirror are spectrally separated at the detector end. The power ratio of these two reflections is insensitive to source fluctuations and fiber-bending loss. However, because the second optical signal depends on the air-gap separation between the end face of the lead-in–lead-out fiber and the reflecting mirror, the ratio provides the information on the air-gap length. A resolution of 0.13 μm has been obtained over a microdisplacement measurement range of 0–254 μm. The sensor is shown to be insensitive to both fiber-bending losses and variations in source power. Based on this approach, a fiber-strain sensor was fabricated with a multilayer interference filter directly fabricated on the end face of the fiber. A resolution of 13.4 microstrain was obtained over a measurement range of 0–20,000 microstrain with a gauge length of 10 mm. The split-spectrum method is also incorporated into a diaphragm displacement-based pressure sensor with a demonstrated resolution of 450 Pa over a measurement range of 0–0.8 MPa.

1. Introduction

Optical fiber sensors have been developed during the past 15 years to measure a wide range of physical observables.[1] Fiber sensors may be divided into two general classes, interferometric devices that measure differential phase changes in multipath fiber geometries and intensity-based devices that measure environmentally induced changes in received optical power. Although a high resolution of phase detection, of the order of 10^{-6} rad, can be obtained with fiber interferometers, they require relatively complicated signal-processing techniques for effective signal recovery. Such signal-processing complexity greatly increases the cost and makes interferometric sensors unacceptable for many applications. Intensity-based fiber sensors conversely require only simple signal processing, while possessing all the obvious advantages of fiber sensors over conventional electric sensing techniques. These advantages include immunity from electromagnetic interference, small size, geometric flexibility, and the possibility of use in harsh environments.

However, because the values of the measurands are directly derived from changes in light intensity for intensity-based sensors, these sensors are especially susceptible to power fluctuation of the light source, fiber loss, and variations in modal power distribution (MPD) in fibers. All these factors cause changes in the output of the sensor that may be misinterpreted as changes in the value of the measurand. The compensation of these changes, usually seen as long-term drift, is therefore a major concern when one is designing an intensity-based sensor system. A considerable amount of research has been conducted in this area in the past few years. In 1983 Giles and coworkers demonstrated a com-

The authors are with the Fiber & Electro-Optics Research Center, Bradley Department of Electrical Engineering, Virginia Polytechnic Institute and State University, Blacksburg, Virginia 24061-0111.

Received 22 June 1995; revised manuscript received 15 January 1996.

0003-6935/96/152595-07$10.00/0

pensation bridge concept using two light sources of the same wavelength.[2] Over a large range of fiber-loss variations, an accuracy of 1% was achieved. In 1984 Jones and Spooncer proposed a two-wavelength referenced technique for grating-type modulators.[3] In 1987 Wang *et al.* proposed a single-wavelength compensation technique for extrinsic polarization-modulated fiber sensors.[4] A long-term accuracy of 0.2% was obtained for multiyear *in situ* field testing.[5] Recently, fiber Bragg grating sensors have been demonstrated for measurement of strain or temperature,[6] for either of which the method of direct wavelength-shift demodulation could be used to extract measurand information. Because such sensors have the advantages of small size, low cost of fabrication, and stable operation, they have been shown to be especially attractive, even though their cross sensitivity for measurements of temperature and strain is still a problem. Also, there have been a variety of other self-referencing techniques with similar objectives proposed by different researchers in recent years.[1] This paper presents a split-spectrum intensity-based (SSIB) sensor approach that permits compensation for both fiber loss and source fluctuation. Three sensors using the SSIB approach for measurements of microdisplacement, strain, and pressure are constructed, and experimental results are presented.

2. Principle of Operation

Figure 1 shows the geometry of the SSIB sensor. The output of a broadband source is coupled into a multimode fiber and propagates through a 2×2 fiber coupler and mode scrambler to the sensor. The short-wave-pass interference edge filter, which is attached to or directly fabricated on the output end face of the lead-in–lead-out optical fiber, reflects the portion of the spectrum above its cutoff wavelength but allows the portion of the spectrum below its edge wavelength to transmit. The reflected signal, referred to as the reference signal, returns directly to the fiber. The light transmitted through the filter, referred to as the sensing signal, propagates across the air gap to the mirror. The light is reflected by the mirror and is then partially recoupled into the fiber. The two reflections travel along the same fiber to the detector end and are separated spectrally by the wavelength division multiplexer (WDM) or demultiplexer. The function of the mode scrambler is to ensure similar MPD's for the two signals. The intensity of the reference signal is independent of the air gap in the sensor, but the intensity of the sensing signal is a function of the air-gap separation. The power ratio of the sensing signal to the reference signal is thus a function of the air-gap separation. However, because the two signals travel along the same optical path in the fiber and are also radiated from the same source, they carry the same information concerning the fiber losses and source-power fluctuations. The power ratio should therefore be immune to variations in both the fiber losses and the source power. Thus a low drift and a high long-term accuracy may be expected for this system.

3. Theory

As described above, the sensor behaves as a fiber-to-fiber junction with a doubled longitudinal air-gap separation. In order to evaluate the excess loss of a fiber splice with a longitudinal separation, we must know the cross-sectional optical intensity distribution outside the input fiber end face. For a single-mode fiber, a Gaussian function gives a good approximation for this intensity distribution.[7] But for a multimode fiber, the optical intensity distribution outside the output fiber end face is contributed by all guiding modes in the fiber, and hence a different MPD leads to a different cross-sectional intensity profile outside the fiber end face. So, in general, to obtain an exact expression for an intensity profile, the phases and amplitudes of the electric fields for all the guiding modes must be known, and then the electric field at any point outside the fiber end face can be derived by the use of Kirchhoff diffraction theory.[8] It is, however, extremely difficult to know exactly the phases and amplitudes of all the guiding modes in a fiber supporting a large number of modes.

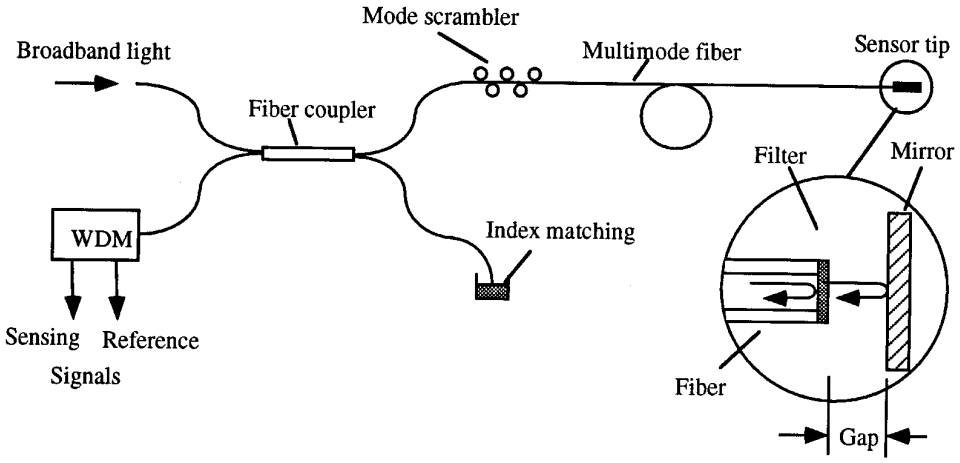

Fig. 1. Schematic of a loss-compensated fiber sensor for displacement measurement. WDM, wavelength division multiplexer.

A number of simplified analytical models for evaluation of the excess loss of step-index multimode fiber splices have been proposed in the past.[9–11] However, because of the complexity of the MPD, only two specific MPD's, namely a uniform MPD and a steady or equilibrium MPD, typically are considered in these models. The model in which a uniform MPD is assumed has a very simple expression.[9] However, it does not describe the behavior of fiber connectors well. Usually, numerical computer simulation is required, with the assumption of a steady MPD. Therefore we try to develop a simple model to describe our sensors.

For normal input excitation conditions, the cross-sectional optical intensity distribution outside the output end face of a step-index multimode fiber has an on-axis central maximum value and an off-axis distribution that decreases with the increase of the radius coordinate away from the axis. This characteristic of the intensity distribution remains true within a relatively large range of varying excitation conditions.

We assume that the cross-sectional optical intensity distribution at any distance outside the output end face of a step-index multimode fiber, as shown in Fig. 2, can be expressed by a Gaussian function in a cylindrical coordinate system as

$$I = I_0 \exp\left\{-A \frac{\rho^2}{[f(z)]^2}\right\}, \tag{1}$$

where ρ is the radius coordinate, I_0 is the intensity at the center of a cross-sectional plane at distance z, and A is a constant related to the MPD in the fiber. The total power in such a plane should be a constant. Thus we have at any distance z

$$P_0 = \int_0^{2\pi} d\Phi \int_0^{\infty} I \rho d\rho. \tag{2}$$

Substituting Eq. (1) into Eq. (2), we obtain

$$P_0 = \frac{\pi}{A} [f(z)]^2 I_0(z). \tag{3}$$

So

$$I_0 = \frac{AP_0}{\pi[f(z)]^2}. \tag{4}$$

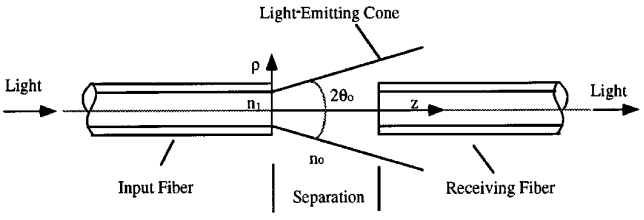

Fig. 2. View of a step-index multimode optical fiber splice with a longitudinal gap separation.

Let us discuss the possible form of function $f(z)$. According to the ray-optics explanation of propagation in a multimode optical fiber, the spatial extent of the light beams out of the fiber is limited to within the emitting cone determined by the numerical aperture of the fiber, as shown in Fig. 2. That means that most of the optical power radiated from the fiber end face is confined within that cone. Naturally we assume that the function $f(z)$ is given by

$$f(z) = z \tan[\sin^{-1}(\mathrm{NA}/n_0)] + a, \tag{5}$$

where a is the radius of the fiber core, NA is the numerical aperture of the fiber, and n_0 is the refractive index of the medium outside the fiber end face. Combining Eqs. (1) and (5), we find that the normalized optical intensity I/I_0 becomes $\exp(-A^2)$ at a radial position $\rho = Z \tan[\sin^{-1}(\mathrm{NA}/n_0)] + a$. So the constant A gives an indication of the amount of optical power within the light-emitting cone, which is related to the MPD. Substituting Eq. (4) into Eq. (1), we obtain the expression of the optical intensity at any point outside the fiber output end face as

$$I = \frac{P_0}{\pi[f(z)]^2} \exp\left[-A \frac{\rho^2}{[f(z)]^2}\right]. \tag{6}$$

In a step-index multimode fiber splice with a longitudinal gap separation, we assume that all the power projected onto the core region of the same type of receiving fiber will be captured. The power entering the fiber can then be written as

$$P = (1 - C) \int_0^{2\pi} d\phi \int_0^{a} I \rho d\rho, \tag{7}$$

where C represents the Fresnel reflection at the end face of the receiving fiber. Substituting Eqs. (5) and (6) into Eq. (7) and considering the condition that when $z = 0$, P must equal $(1 - C)P_0$, we thus obtain the power collected by the receiving fiber of the splice as

$$P = (1 - C)P_0\left[1 + \exp(A) - \exp\left(-\frac{Aa^2}{[z \tan[\sin^{-1}(\mathrm{NA}/n_0)] + a]^2}\right)\right], \tag{8}$$

where z represents the longitudinal gap separation between the two fiber end faces.

Because the behavior of the sensor element can be considered equivalent to that of a fiber splice with a doubled longitudinal gap separation, the sensor output can be written as

$$R = \frac{P + P_F}{P_{\mathrm{ref}}}, \tag{9}$$

where $P + P_F$ is the total optical power in the sensing

signal, P is described in Eq. (8), and P_F represents the optical power, which is independent of the air-gap variation in the sensor element. The optical power P_F is mainly contributed by the Fresnel reflection of the sensing signal at the air–glass interface at the far end of the filter substrate. P_{ref} is the optical power in the reference signal that is reflected by the interference filter.

4. Experiments

To verify the model described in Section 3, an experiment was performed to measure the excess loss of a step-index multimode fiber splice. In the experiment, a light-emitting diode (LED) at 820 nm pigtailed to a step-index 100/140 μm multimode fiber with a numerical aperture of 0.284 served as the light source. The same type of fiber was used for the coupler and the sensing fiber. In the experiment, the constant A in Eq. (8) was determined to be 4.32 by evaluation of the far-field spatial optical intensity distribution. Figure 3 indicates that a Gaussian function gives a good description of the cross-sectional intensity distribution outside the fiber end face. Figure 4 shows the experimental results of the excess loss of the fiber splice measured versus the longitudinal gap separation. The results presented in Figs. 3 and 4 demonstrate that the model proposed in this paper gives a good description of the excess loss of the step-index multimode fiber splice.

Several sensors based on the SSIB approach were constructed and tested. The first sensor was an intensity-based displacement sensor, as shown in Fig. 1, to test the split-spectrum compensation technique. The target mirror was attached to a micropositioner to permit precise changes in the gap separation. An LED centered at 820 nm with a spectral width of 12 nm was used as the light source. The edge interference filter, deposited on a 0.15-mm-thick glass substrate, with a cutoff wavelength of 820 nm, was selected to match the central wavelength of the LED. The filter was attached to the fiber by the use of index-matching optical epoxy, with the film surface of the filter adjacent to the fiber end face. The mirror, which was mounted on a micropositioner, was adjusted to be perpendicular to the fiber axis. An edge filter identical to the filter used at the sensor head was used to separate the sensing and reference signals at the detectors.

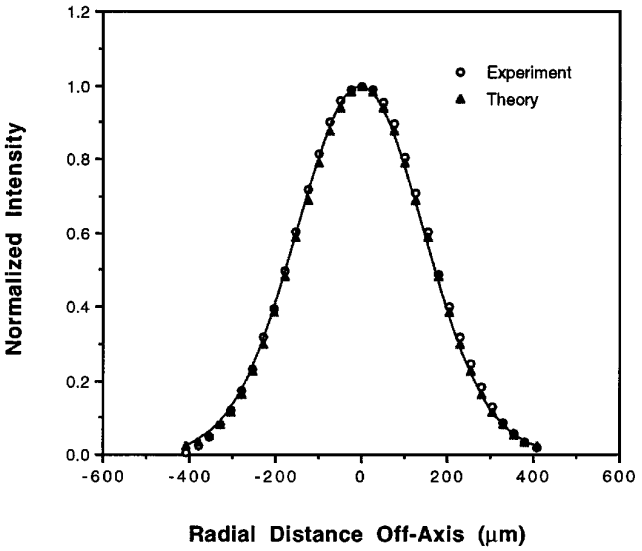

Fig. 3. Cross-sectional intensity profile of the far field at 900 μm from the output end face of the input fiber of the splice.

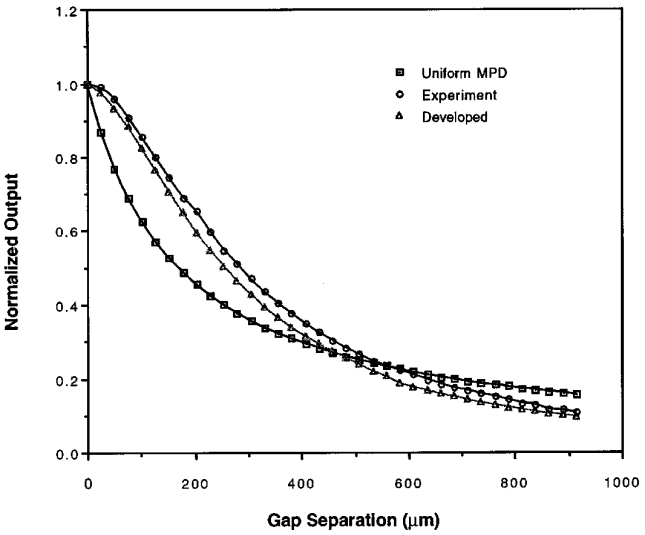

Fig. 4. Optical power in the receiving fiber as a function of the longitudinal gap separation.

The mirror was moved 100 steps in increments of 25.4 μm (0.001 in.), and the ratio of the sensing signal to the reference signal was recorded at each step. For this experiment the output of the sensing-signal detector was 1.82 V without the target mirror. When the gap between the mirror and the filter was set to zero, the output of the sensing-signal detector was 7.8 V. Figure 5 is a plot of the results of the experiment in comparison with the theoretical predictions. The thickness of the filter substrate (150 μm) has been accounted for during this analysis. As can be seen in Fig. 5, the theoretical model closely predicts the experimental SSIB sensor results in a simple displacement sensor configuration. A resolution of 0.13 μm was obtained at the zero point under the detection bandwidth of 2.1 Hz.

Because the sensing and reference signals travel in the same fiber, it is assumed that these two signals should carry the same information about fiber attenuation. However, because the two signals have slightly different MPD's in the fiber, they will experience slightly different optical power variations when the fiber is subjected to bending. Figure 6 presents a plot showing the dependence of the sensor output ratio on the input–output fiber-bending loss. As shown in this figure, the variation of the sensor output ratio remained below 5% for bending losses up to 50% of the total power. The presence of the mode scrambler, located approximately 5 m away from the sensing filter, reduces the

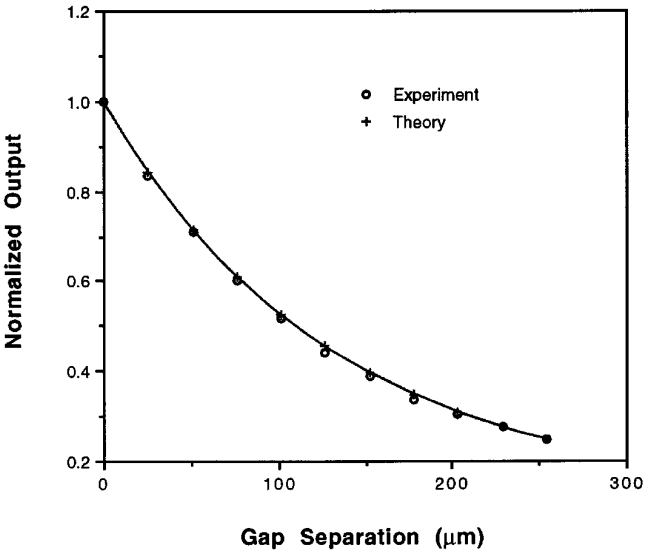

Fig. 5. Sensor output as a function of the longitudinal gap separation.

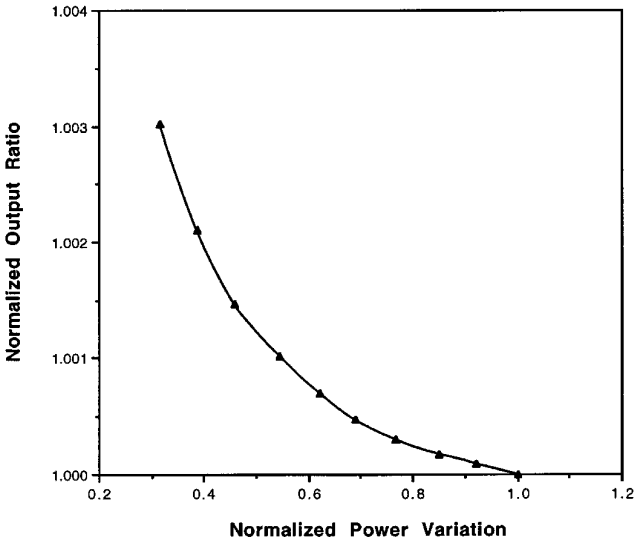

Fig. 7. Dependence of the sensor output on the LED current.

MPD dependence. In experiments, it was found that when the mirror was tilted slightly the sensor output versus the air-gap separation shown in Fig. 5 followed a different curve that was lower than but almost parallel to the original curve. Here it is important to notice that for most practical applications fiber-loss variation, caused by changes in environmental conditions, is usually much smaller than the tested bending-loss variation range. So an accuracy of much better than 5% may be obtained when the sensor is operated under practical conditions.

The results of the experiment performed to measure the dependence of the sensor output ratio versus the input power level are shown in Fig. 7. This graph indicates that the sensor output ratio changes less than 0.2% with LED output power variations of 60%. The LED drive-current variation not only changed the power output, but also moved the central wavelength of the LED. It is believed that this change in wavelength is the factor that caused the small change in the output ratio indicated in Fig. 7. For most applications, the amount of power change shown here is far greater than would be experienced in practical situations. These two tests indicate that the SSIB sensor is capable of compensating for fiber losses and source-power fluctuations.

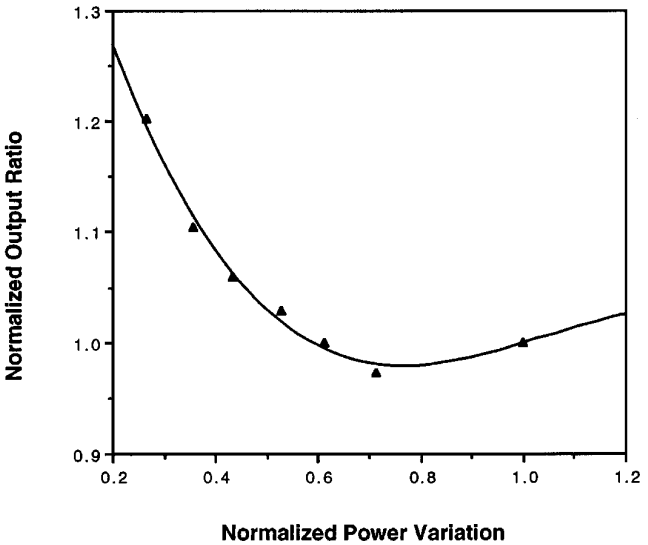

Fig. 6. Dependence of the sensor output on the fiber-bending loss.

The second sensor was fabricated for absolute strain measurement. The sensor is illustrated in Fig. 8. A tungsten halogen lamp served as the light source, which provided a flat spectrum over the spectral region of interest. A 100/140-μm step-index multimode optical fiber served as the lead-in–lead-out fiber and the reflecting fiber. The multilayer dielectric interference filter was directly deposited on the end face of the lead-in–lead-out fiber. The cutoff wavelength of the edge filter was located at 820 nm. A reflecting fiber with an aluminum-coated end face functioned as the reflector. The two fibers were inserted into a hollow glass tube with an inner diameter of 145 μm so that the motion of the fibers could be well guided in the tube. Two wavelengths were selected at the detector end by the use of two bandpass filters at 800 nm and 860 nm, with identical spectral widths of 15 nm. The measured sensor output ratio as a function of strain is plotted in Fig. 9. It can be seen that the sensor output is quite linear over a strain range from 0 to 20,000 με. A resolution of 13.4 με was obtained at the zero point for a detection bandwidth of 2.1 Hz.

The temperature dependence of the sensor was also examined. After the above tests, the sensing and the target fibers were fixed to the hollow glass tube with epoxy. The sensor head was placed in an oven, in which temperature was monitored with a thermocouple. The test result is presented in Fig. 10. The small change in the sensor output is be-

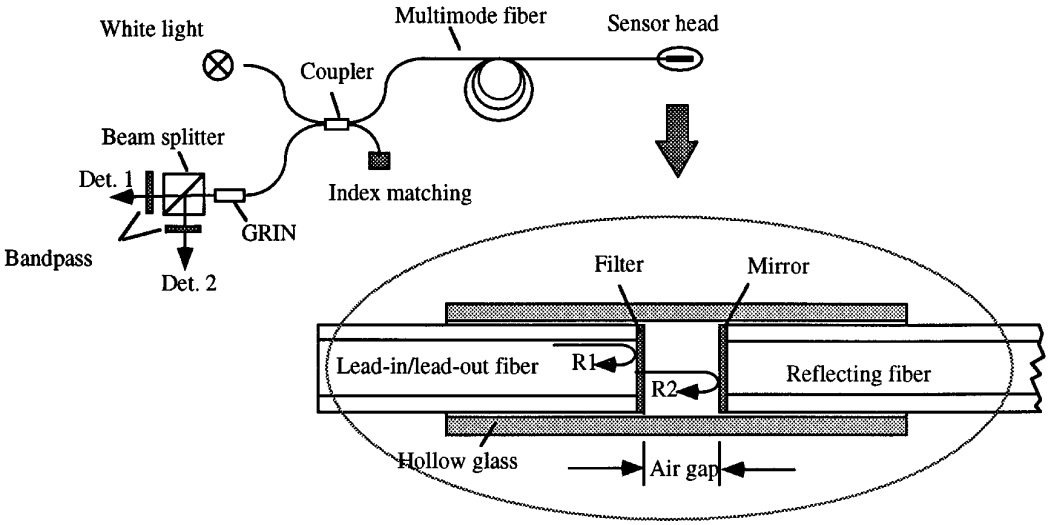

Fig. 8. Configuration of the strain sensor tip. GRIN, graded index.

lieved to be caused mainly by the thermal properties of the epoxy and the differential thermal expansion of the fiber and the hollow glass tube.

Finally, as a further application of the split-spectrum loss-compensated technique, a pressure sensor was fabricated by incorporation of a flat diaphragm functioning as the reflecting mirror. The central displacement of a flat diaphragm can be expressed by[12]

$$y = \frac{0.1706Pr^4}{Eh^3}, \tag{10}$$

where P is the applied pressure, r is the radius, E is the Young's modulus, and h is the thickness. Equation (10) holds for small diaphragm displacements that remain in the elastic range of the material. The pressure-sensor configuration is shown in Fig. 11. The diaphragm was made of stainless steel with a thickness of 0.33 mm and a diameter of 25 mm. For this configuration, the central displacement of the diaphragm was a function of the differential pressure $(P_1 - P_2)$. The output ratio of the sensor is therefore a function of differential pressure.

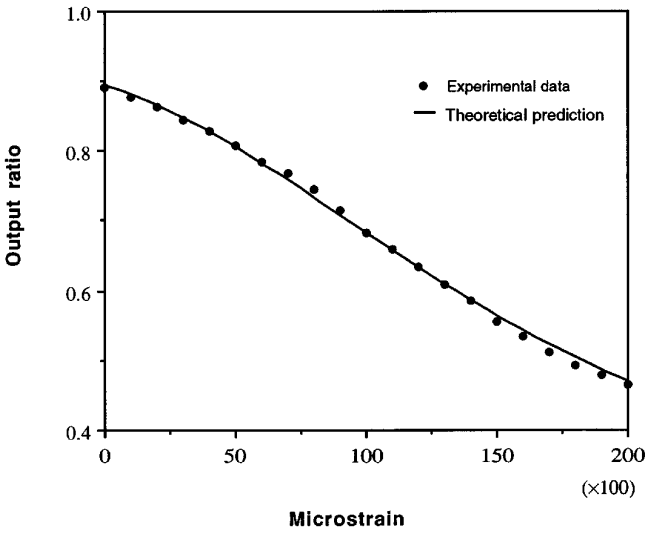

Fig. 9. Output ratio of the sensor as a function of strain.

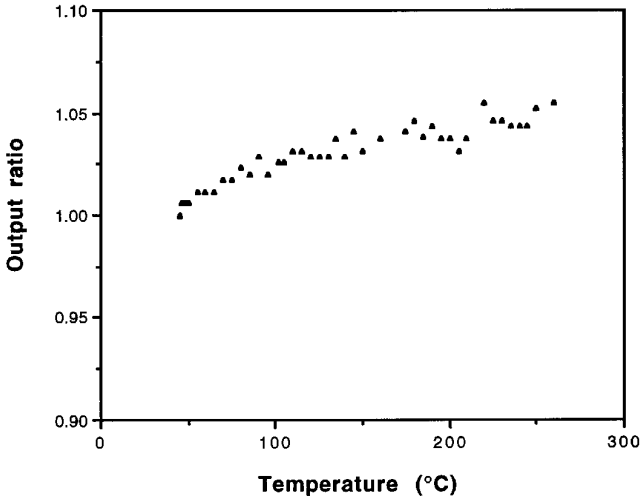

Fig. 10. Temperature dependence of the sensor output.

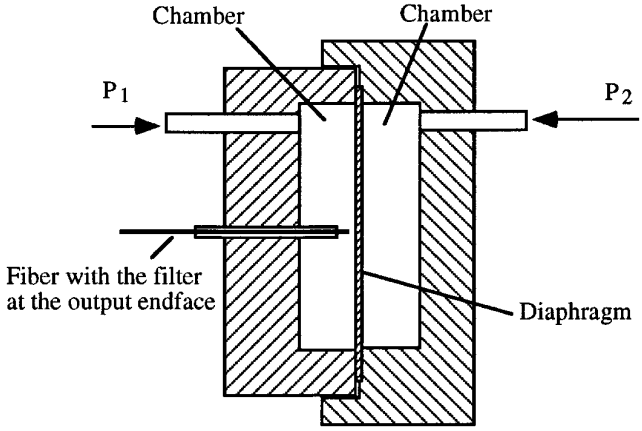

Fig. 11. Schematic of the pressure-sensor head.

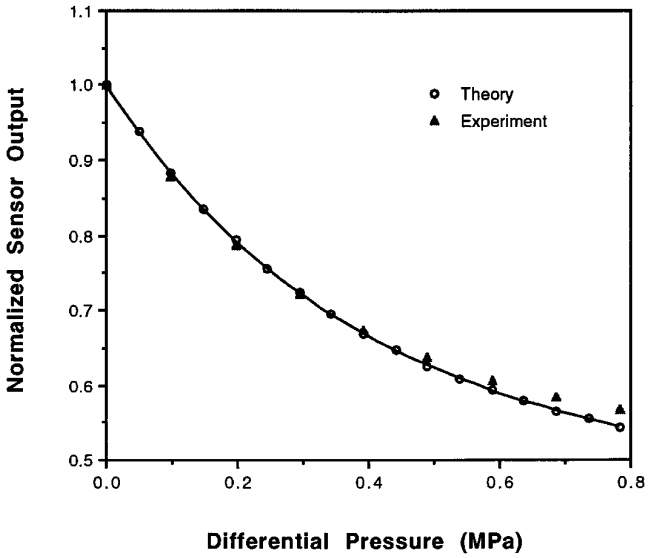

Fig. 12. Output of the pressure sensor as a function of differential pressure.

Figure 12 shows the calibration curve of the sensor as well as the theoretical predictions. A resolution of 450 Pa was achieved, with a measurement range of 0–0.8 MPa.

5. Conclusions

We have demonstrated a split-spectrum compensation technique that permits compensation for fiber-loss variations and source-power fluctuations in air-gap intensity-based fiber sensors. Three sensors for measurements of microdisplacement, strain, and pressure have been constructed and tested. First, for the microdisplacement measurement, a resolution of 0.13 μm has been achieved over a measurement range of 0–254 μm. The sensor has been shown to be immune to source-power fluctuations and fiber-bending losses. Second, a reflective strain sensor was fabricated based on the split-spectrum technique. Experimental testing results have indicated a resolution of 13.4 με over a range of 0–20,000 με. Because of its small geometric dimension, the sensor would be useful for evaluation of embedding materials. Finally, we demonstrated pressure measurements incorporating the compensation technique, in which a diaphragm functions as the reflecting mirror. A resolution of 450 Pa was obtained, with a measurement range of 0–0.8 MPa. A simplified theoretical model has been developed for the description of the sensors. The experimental results agree very well with the theoretical predictions. The method reported here may also be applied to other intensity-based fiber sensors.

The authors thank the Virginia Center for Innovative Technology for initial support to this research. Subsequent work has been supported in part by Fiber and Sensor Technologies, Inc.

References

1. E. Udd, *Fiber Optic Sensors—An Introduction for Engineers and Scientists* (Wiley, New York, 1991).
2. I. P. Giles, S. McNeill, and B. Culshaw, "A stable remote intensity based fiber sensor," J. Phys. E **18,** 1124–1126 (1985).
3. B. E. Jones and R. Spooncer, "An optical fiber pressure sensor using a holographic shutter modulator with two wavelengths intensity referencing," in *Second International Conference on Optical Fiber Sensors: OFS'84,* R. T. Kersten and R. Kist, eds., Proc. SPIE **514,** 223–226 (1984).
4. A. Wang, J. Lin, S. He, B. Wu, and W. Wu, "Compensation technique for polarimetric fiber optic sensors," patent 8526 (China, 1987).
5. A. Wang, S. He, X. Fang, X. Jin, and J. Lin, "Optical fiber pressure sensor based on photoelasticity and its applications," IEEE J. Lightwave Technol. **10,** 1466–1471 (1992).
6. W. W. Morey, G. Meltz, and W. H. Glenn, "Fiber optic Bragg grating sensors," in *Fiber and Laser Sensors VII,* R. P. DePaula and E. Udd, eds., Proc. SPIE **1169,** 98–107 (1989).
7. F. C. Allard, *Fiber Optics Handbook* (McGraw-Hill, New York, 1990), Chap. 3.
8. M. Born and E. Wolf, *Principles of Optics: Electromagnetic Theory of Propagation, Interference and Diffraction of Light,* 6th ed. (Pergamon, London, 1975), pp. 375–382.
9. G. Keiser, *Optical Fiber Communications,* 2nd ed. (McGraw-Hill, New York, 1991), p. 214.
10. M. J. Adams, D. N. Payne, and F. M. E. Sladen, "Splicing tolerances in graded-index fibers," Appl. Phys. Lett. **28,** 524–526 (1976).
11. C. M. Miller and S. C. Mettler, "A loss model for parabolic profile fiber splices," Bell Syst. Tech. J. **57,** 3167–3180 (1978).
12. M. Di Giovanni, *Flat and Corrugated Diaphragm Design Handbook* (Dekker, New York, 1982).